Journal of
Composites Science

MDPI

Article

Finite Element Multi-Physics Analysis and Experimental Testing for Hollow Brick Solutions with Lightweight and Eco-Sustainable Cement Mix

Matteo Sambucci [1,2,*], Abbas Sibai [1], Luciano Fattore [3], Riccardo Martufi [3], Sabrina Lucibello [3,4] and Marco Valente [1,2]

[1] Department of Chemical Engineering, Materials, Environment, Sapienza University of Rome, 00184 Rome, Italy; abbas.sibai@uniroma1.it (A.S.); marco.valente@uniroma1.it (M.V.)
[2] INSTM Reference Laboratory for Engineering of Surface Treatments, Department of Chemical Engineering, Materials, Environment, Sapienza University of Rome, 00184 Rome, Italy
[3] Center for Research and Services Saperi&Co, Sapienza University of Rome, 00185 Rome, Italy; luciano.fattore@uniroma1.it (L.F.); riccardo.martufi@uniroma1.it (R.M.); sabrina.lucibello@uniroma1.it (S.L.)
[4] Department of Planning, Design, Technology for Architecture, Sapienza University of Rome, 00196 Rome, Italy
* Correspondence: matteo.sambucci@uniroma1.it; Tel.: +39-06-44585647

Abstract: Combining eco-sustainability and technological efficiency is one of the "hot" topics in the current construction and architectural sectors. In this work, recycled tire rubber aggregates and acoustically effective fractal cavities were combined in the design, modeling, and experimental characterization of lightweight concrete hollow bricks. After analyzing the structural and acoustic behavior of the brick models by finite element analysis as a function of the type of constituent concrete material (reference and rubberized cement mixes) and hollow inner geometry (circular- and fractal-shaped hollow designs), compressive tests and sound-absorption measurements were experimentally performed to evaluate the real performance of the developed prototypes. Compared to the traditional circular hollow pattern, fractal cavities improve the mechanical strength of the brick, its structural efficiency (strength-to-weight ratio), and the medium–high frequency noise damping. The use of ground waste tire rubber as a total concrete aggregate represents an eco-friendlier solution than the ordinary cementitious mix design, providing, at the same time, enhanced lightweight properties, mechanical ductility, and better sound attenuation. The near-compliance of rubber-concrete blocks with standard requirements and the value-added properties have demonstrated a good potential for incorporating waste rubber as aggregate for non-structural applications.

Keywords: ground waste tire rubber; hollow concrete brick; fractal; finite element analysis; compressive strength; acoustic absorption; eco-sustainability

Citation: Sambucci, M.; Sibai, A.; Fattore, L.; Martufi, R.; Lucibello, S.; Valente, M. Finite Element Multi-Physics Analysis and Experimental Testing for Hollow Brick Solutions with Lightweight and Eco-Sustainable Cement Mix. *J. Compos. Sci.* **2022**, *6*, 107. https://doi.org/10.3390/jcs6040107

Academic Editor: Krishanu Roy

Received: 23 March 2022
Accepted: 2 April 2022
Published: 5 April 2022

1. Introduction

Our dependence on waste tires is clear; just think of the world of transport, in general. About 800 million tires worldwide reach their end of life each year, and much of the rubber from which they are made, which represents about 50% of their weight, is lost [1]. To effectively close the waste management cycle in a circular economy view, such material can be recycled as a granular product and intended for civil engineering applications. The key markets for material recovery are as follows [2]: (1) whole tires used to fabricate crash barriers, bumpers, or artificial reefs; (2) crumb rubber used to produce molded rubber products, flooring, or matting; and (3) powdered rubber used as modifiers to asphalt paving mixtures. During the last three decades, researchers investigated the possible use of ground waste tire rubber (GWTR) in concrete and mortars. Since the pioneering study on engineering properties of rubberized concrete conducted by Eldin and Senouci [3] in the

1990s, a large number of research activities have taken place, proving the possibility of creating alternative and eco-sustainable cementitious mixes, thanks to the presence of rubber particles recovered from discarded tires that replace the ordinary virgin aggregate. Besides the environmental benefits, the researchers suggested that cement-based composites incorporating GWTR can significantly enhance toughness and energy absorption [4], increase the mechanical strain capacity [5], achieve better noise attenuation performance [6,7], raise thermal insulation capacity [8], and improve freeze–thaw resistance with entrapped air voids [9] compared to plain concrete. However, it is also well documented that replacing the ordinary aggregates (sand and gravels) with GWTR adversely affects the concrete's mechanical properties, such as static stiffness and compressive strength, which can limit its use in structural applications [10,11].

The literature survey above shows that there is a potential for the use of rubber aggregates in building/architectural elements where the primary requirement is not mechanical strength but lightweight, thermal–acoustic efficiency, and durability, such as hollow bricks. Brick is the most basic precast unit for the construction of low-cost houses and multi-stored apartments. There are remarkable and noteworthy points going in favor of the use of these hollow components [12]:

- The dead load is much lower than for a solid block; due to this, one can structurally engineer them and reduce steel consumption in construction;
- The heat insulation of wall structures is achieved due to the inner cavities, which provide energy saving for all times. Similarly, hollowness results in improved sound attenuation;
- Low maintenance cost, minimal material requirements, and cost competitiveness with other materials make it a preferred material for today's building.

The conventional type of brick is made of fired clay [13]. Clay brick manufacturing is an energy-intensive process. It involves the consumption of a considerable amount of energy during the firing process, requiring temperatures between 1000 and 1200 °C, depending on the raw materials [14]. Apart from providing the above-listed features, rubber-concrete hollow bricks could eliminate this drawback, since no fuel and thermal treatment are necessary for their production. Except for the clinkering concerning the production of the cement binder, the curing and hardening of concrete bricks takes place at room temperature, without involving firing or other additional processing. At the same time, the presence of recycled rubber aggregates would bring valuable benefits from both an environmental and a technological point of view. Some attempts aimed at the design, development, and characterization of GWTR-added bricks were made in the past few years. Turgut and Yesilata [13] investigated the physical–mechanical and thermal performance of rubberized solid brick with varying sand-crumb rubber volumetric replacement (from 10% *v/v* to 70% *v/v*). The thermal insulation performances of these bricks are found to be better than their ordinary counterpart (percentage-wise insulating improvements up to 11%), and the mechanical properties of the samples satisfied the requirements reported in the international technical standards. Mohammed et al. [15] developed hollow concrete blocks by using 0% *v/v*, 10% *v/v*, 25% *v/v*, and 50% *v/v* GWTR as a replacement for fine mineral aggregate. The authors discovered that the samples can be produced as load-bearing hollow blocks, as well as lightweight hollow blocks, providing better thermal and acoustic performance in comparison with conventional hollow blocks. Fraile-Garcia et al. [16] examined the acoustic behavior of hollow bricks made of concrete doped with waste tire rubber (0%, 20%, and 30%). Elements with the maximum percentage of rubber in their composition provided a better response than the control samples (0% rubber) for low-frequency noise, both in the case of airborne insulation and impact sound insulation. In the first case, the improvement was up to 50%, whereas, in the second case, this percentage was 15%. Therefore, highly rubber-modified construction elements are convenient to isolate the low-frequency sounds, such as instruments or road traffic vehicles (heavy trucks, tractors, etc.) emissions. Al-Fakih et al. [17] analyzed the mechanical performance of interlocking masonry walls that were constructed using rubberized hollow bricks (10% *v/v* of crumb

rubber). In contrast to conventional masonry walls under compressive loading, GWTR–cement interlocking walls showed increased ductility, experiencing measurable post-failure loads with significant displacement, due to the presence of crumb rubber, which allows for a large expansion of microcracks inside the specimens after failure.

Complementary to the material's composition, the internal geometry of the brick units assumes a crucial role in its structural, thermal, and acoustic performance [18]. Supported by digital design and finite-element modeling tools, several researchers were involved in studying optimized internal cavities to improve specific performance characteristics of the hollow bricks. A collection of some works on this research topic is reported in Table 1.

Table 1. Design and shape optimization of hollow concrete bricks: A brief overview.

Research Work	Aim of the Study	Major Remarks
Del Coz Díaz et al. [19]	Topological optimization of twelve hollow concrete block units, varying the number and shape of inner recesses, with the aim of reducing the brick's weight, keeping suitable structural properties.	A weight reduction close to 45% is obtained with respect to the classic concrete block, keeping comparable structural efficiency in terms of strength-to-weight ratio.
Al-Tamimi et al. [20]	Twenty-three brick designs with different hole arrangements and one solid model were studied for concrete material to reach the model with the optimum holes in terms of thermal-insulation efficiency.	Increasing the hollow ratio tends to decrease the heat transfer from outer to inner brick sides significantly. At the same hollow ratio, there was an effect of the shape of holes in reducing the thermal flow through the bricks: rectangular shapes were more thermo-effective than circular ones.
Sassine et al. [21]	Mechanical and thermal behaviors of ten concrete hollow-block configurations are simultaneously studied by varying the blocks' internal shape, aiming at determining the optimal hollow-block design and providing the optimal compromise between thermal insulation and mechanical strength.	Longitudinal bulkheads improve the thermal resistance of the blocks and, thus, reduce the heat flux passing through the element. The mechanical behavior varies slightly between the investigated models in vertical compression, reducing the influence of this parameter in the selection of the best design.
Valente et al. [22]	Mechanical performance of three types of hollow-brick designs, circular, square, and hexagonal holes, were numerically analyzed to select the best configuration for rubber–concrete mixes.	Circular and hexagonal hole designs offer the best result in terms of compressive strength. The "honeycomb" geometries have remarkable thermal and acoustic functionality; therefore, they have more attractive requirements for building.

There are a very limited number of works investigating functional brick configurations in terms of acoustic performance, which is one of the primary requirements in the design of building elements. Noise control has become an imperative engineering field in modern society, not only because of the recent recognition of noise as a serious health hazard, but also because the standard of living and the quality of life are becoming more important [23].

This study is focused on investigating the performance of GWTR–cement bricks topologically engineered with inner hollow layouts potentially designed for sound attenuating applications. Specifically, the influence of easy-to-design-and-manufacture fractal cavi-

ties was analyzed by finite element analysis (FEA), experimentally tested, and compared with hole shapes (circular) commonly used in brick technology. Fractal geometries were extensively studied in anti-noise applications, such as acoustic damping cavities for sound-absorbable systems based on Helmholtz's resonators [24–26]. Highly irregular cavity shapes increase the viscous resistance at the cavity boundary by adding geometrical features that impede the natural direction of airflow. Consequently, the sound wave, interacting with the cavity, experiences significant dissipation phenomena [26]. The key purpose of the present research was to model, develop, and characterize brick prototypes with double technological functionality, which means, deriving both from the rubberized concrete's characteristics (lightweight, toughness, thermo-acoustic peculiarities, eco-friendliness) and the component's design. The manuscript is structured in three parts:

- *Part 1*—Description and key properties of the cement mixes (reference and rubberized concretes) used for hollow bricks manufacturing;
- *Part 2*—Design, topological optimization, and finite element modeling (mechanical and acoustic analysis) of hollow brick prototypes based on circular and fractal inner cavities;
- *Part 3*—Production process of the designed hollow bricks, mechanical and acoustic experimental characterization, and FEA models validation.

2. Materials and Methods

2.1. Part 1: Raw Materials and Concrete Mixes Characterization

2.1.1. Raw Materials

Constituent materials for concrete mixes included a commercial Type II Portland limestone cement (strength class 42.5 R) supplied by Colacem (Gubbio, Italy), fine river sand, and GWTR aggregates. Two fractions of recycled tire rubber particles, 0–1 mm rubber powder (RP) and 1–3 mm rubber granules (RG), were provided by the European Tyre Recycling Association (ETRA, Brussels, Belgium) and manufactured by ambient mechanical shredding processing of waste tires. The polymeric aggregates were used to produce the rubber–cement mix as a volumetric replacement of the mineral aggregate. The river sand and GWTR particles involved in this research work are presented in Figure 1.

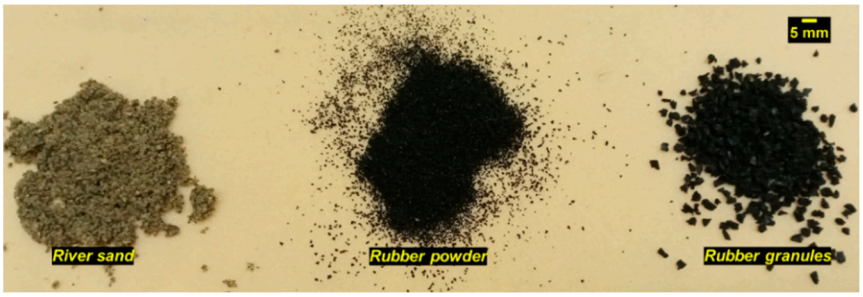

Figure 1. River sand and GWTR used in this study.

The density of the aggregates was measured by the pycnometer method. For sand, water was employed as a test fluid, in agreement with the EN 1097-7 [27] standard method. Concerning the testing on rubber, the standard protocol was slightly modified, employing denatured ethylic alcohol (Deterchimica, Viterbo, Italy) as a fluid of known density to minimize undesired floating phenomena. The water absorption was assessed as the ratio of the difference between the weight of the aggregates in saturated surface dry (SSD) condition and oven-dry condition (110 °C for 24 h) to the weight of oven-dry aggregates. The physical properties of the mineral and GWTR aggregates are shown in Table 2.

Table 2. Physical properties of river sand and GWTR.

Aggregate	Density (kg/m^3)	Water Absorption (%)
River sand	2476	20.0
GWTR	1144	9.6

Figure 2 presents the size-grading analysis of rubber particles and sand, determined via the vibrating sieving method, following the DIN 51701 [28] standard.

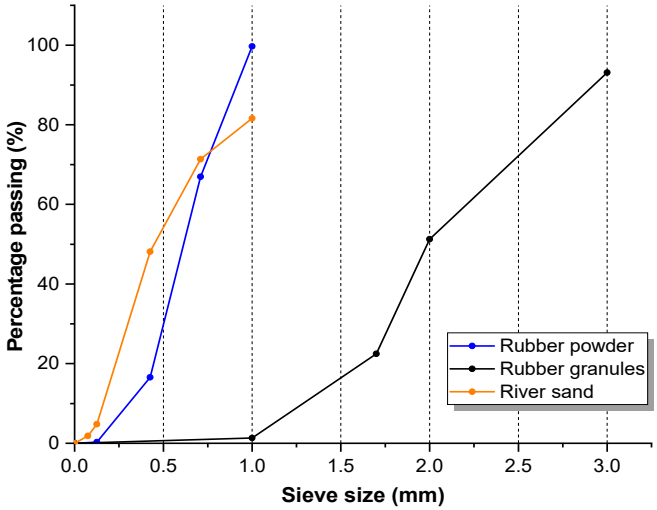

Figure 2. Particle size distribution of RP, RG, and river sand.

2.1.2. Mix Proportions and Samples Preparation

In this research, a single rubber–cement formulation (designed as RuC) that was obtained by totally replacing the sand with the two rubber fractions was investigated to produce the brick prototypes. Specifically, the mix design incorporated fine and coarse polymer aggregates in equal proportion (50% *v/v* RP–50% *v/v* RG). Such selected GWTR dosage was determined as "optimum" in previous research works conducted by the authors, where the influence of the tire aggregate size on the physical, mechanical, and microstructural performances of 3D printable cement [29,30] mixes and rubberized alkali-activated composites [31] was investigated in detail.

Reference concrete mix (REF), involving 0% *v/v* of GWTR, was also produced for comparison purposes. For REF mix, a water-to-cement ratio of 0.42 was chosen in agreement with common technical requirements to ensure proper cement mass hydration. In the rubberized formulation, the water dosage was adjusted to achieve proper fluidity and workability for mold-casting. The mix proportions of investigated formulations are listed in Table 3.

Table 3. Concrete mix proportions.

Sample ID	Cement (kg/L)	Water (kg/L)	Sand (kg/L)	RP (kg/L)	RG (kg/L)	w/c Ratio
REF	0.72	0.300	1.20	/	/	0.42
RuC	0.72	0.325	/	0.275	0.275	0.45

Dry components (cement, sand, and GWTR) were mixed inside a plastic tank to achieve a homogeneous blend. Tap water was gradually added to the mix until an adequate fluidity level for the pouring of the hydrated compound into the mold was reached. During the water addition, the batch was subjected to some vibration cycles, by a Giuliani IG/3

shaker machine (Giuliani Tecnologie, Turin, Italy), to improve the constituent mixing. Then the fresh mix was cast into rectangular plastic molds (110 mm × 185 mm × 50 mm). After casting, an additional vibration operation (2 min) was performed to expel any air bubbles embedded during the mixing and pouring. Firstly, the samples were cured in air for 24 h, and then the semi-hardened slabs were extracted from the molds and cured underwater for 28 days. After curing, for each concrete mix, a series of specimens were collected (Table 4) by wet sawing with an abrasive cutting disk, and they were intended for experimental testing. The materials characterization, described in detail below, provided the main physical, mechanical, and acoustic properties of the formulations under examination to be used as input data for the FEA analysis.

Table 4. Test samples for materials characterization.

Specimen Type	Number of Specimens per Test	Test
1 cm^3 cubes	3	Density
1 cm^3 cubes	3	Permeable porosity
1.5 cm × 1.5 cm × 10 cm beams	3	Three-point flexural test
1.5 cm × 1.5 cm × 3 cm prisms	3	Compressive test
5 cm × 5 cm × 2.5 cm blocks	1	Acoustic flow resistivity

2.1.3. Testing Program and Experimental Results

The density (ρ) of each specimen was measured by the hydrostatic weighing method described in ASTM D792 standard [32], using a ME54 analytical balance (Mettler Toledo, Columbus, OH, USA) equipped with a kit for gravimetric measurements.

The permeable porosity (Φ) was evaluated by vacuum saturation technique (ASTM C1202 standard [33]), using the experimental setup and test conditions presented in Figure 3a.

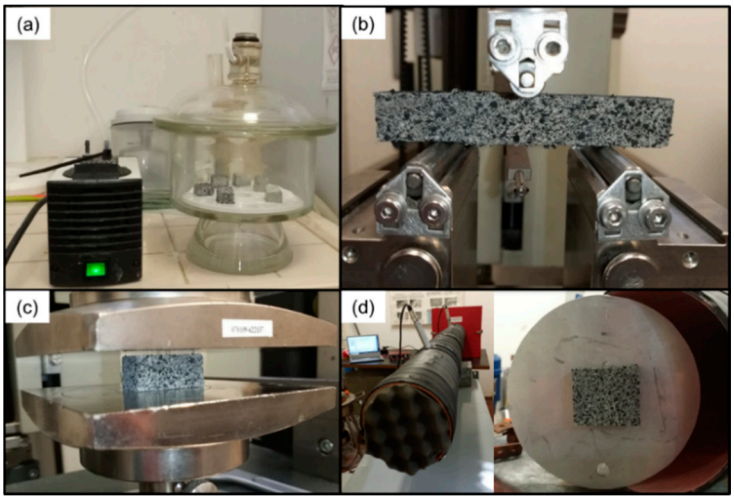

Figure 3. Graphical overview of the experimental program for materials characterization: (**a**) vacuum saturation method, (**b**) three-point flexural test, (**c**) compressive test, and (**d**) acoustic flow resistivity measurement.

The mechanical behavior of the samples was studied under flexural and uniaxial compression, using a Zwick-Roell Z10 (Zwick-Roell Group, Ulm, Germany) universal machine equipped with a 10 kN load cell. The bending test was performed in a three-point configuration (Figure 3b) with a support span of 60 mm, a cross head speed of 1 mm/min, and a pre-load of 5 N. Compressive test (Figure 3c) was run at 1 mm/min in displacement control. Flexural tensile strength (σ_t), compressive strength (σ_c), and compressive elastic

modulus (E_c) were recorded and analyzed with TestXpert II software (Zwick-Roell Group, Ulm, Germany).

Measurements of the acoustic flow resistivity (R_f) were executed in an impedance tube (Figure 3d) in accordance with the test method proposed by Ingard and Dear [34]. More detailed information about the experimental setup can be found in Reference [35].

Table 5 provides the experimental results for ρ, Φ, σ_f, σ_c, E_c, and R_f of REF and RuC concrete mixes, including the average values with the standard deviation in brackets.

Table 5. Concrete mix proportions.

Sample ID	ρ (kg/m^3)	Φ (%)	σ_t (MPa)	σ_c (MPa)	E_c (GPa)	R_f (N × s × m^{-4})
REF	2186 (18)	21.39 (0.25)	11.06 (1.48)	35.89 (7.71)	1.62 (0.47)	13,872
RuC	1281 (21)	22.82 (0.37)	1.65 (0.51)	4.93 (0.57)	0.24 (0.02)	19,862

The unit weight, mechanical strength, and stiffness of RuC mix were expected to be less than that of REF sample. The decrease is mainly attributed to the replacement of sand with lightweight polymer aggregates, the difference in deformability between rubber and cement paste that generates high-stress concentration at the interfacial transition zone (ITZ), leading to the formation of cracks in that region, the weak bonding between GWTR and cement matrix, and the entrapped air from the hydrophobic rubber particles, assisting the generation of internal porosity in the hardened material [36]. Although the addition of rubber would lead to an increase in the air void rate, experimental Φ-values demonstrated similar characteristics between REF and rubberized mixes. The proportion ratio between fine and coarse rubber fractions selected in this research provided beneficial effects in terms of microstructural properties. In this regard, some researchers have verified that incorporating varying sizes of GWTR improved the aggregate gradation so that a denser microstructure is produced to decrease the material's permeability [37,38]. R_f data showed a clear improvement in the acoustic properties of the cementitious mix by replacing the sand with the rubber fractions. GWTR aggregates would provide an additional sound attenuation mechanism related to their viscoelastic nature. When the rubber aggregate is vibrated, part of the energy is stored (elastic) and part is dissipated as heat (viscous) within the polymer. This viscous property results in loss of vibration energy as heat rather than being radiated as noise [39].

2.2. Part 2: Design, Modeling, and FEA of Hollow Bricks

COMSOL Multiphysics (COMSOL Inc., Stockholm, Sweden) computer aid engineering (CAI) software was employed for designing the hollow brick prototypes and modeling via FEA and their mechanical and acoustic behavior as a function of constituent concrete mix (REF and RuC mixes) and holes configuration.

2.2.1. Hollow Bricks Design

At first, COMSOL Multiphysics 3D geometry tool was used to design the brick models. The investigated models had the same dimension: rectangular base of 110 mm × 170 mm and height of 50 mm. Two different inner cavity designs were studied: circular hollow design (CHD) and fractal hollow design (FHD). Regarding the fractal design, a geometric configuration of easily modeling and manufacturing was investigated, so it could feasibly be scaled in brick prototype manufacturing. In this regard, the second-order Minkowski structure (Figure 4) was selected to produce the fractal pattern. This type of geometry was successfully implemented by the authors in previous research work for the development of acoustically active cavities in polymeric Helmholtz resonator prototypes intended for sound-absorbing interventions in automotive [40].

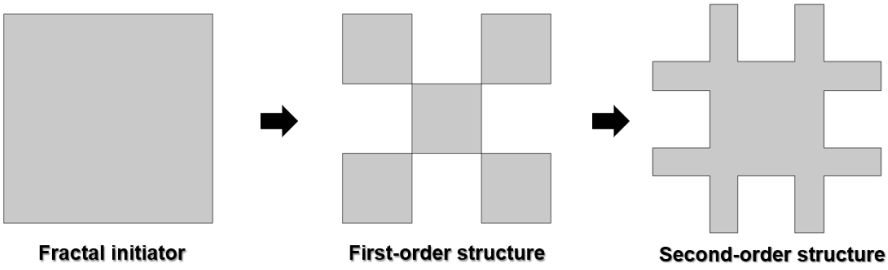

Figure 4. Iterative generation of the second-order Minkowski fractal geometry.

The size and number of the holes were defined in accordance with the technical indications reported in EN 771-1 standard [41] for half-solid bricks, considering a hole concentration ratio of 20–30%. The reference standard defines the specific design requirements as follows:

1. Hole area <1200 mm^2;
2. Minimum hole-external-perimeter distance >15 mm;
3. Minimum distance between adjacent holes >8 mm.

By adopting the above-reported design constraints, the circular and fractal cavities were arranged in the brick models, following a "honeycomb" pattern. Nagy and Orosz [42] demonstrated that this type of cavity arrangement extends the trajectory of the thermal flow inside the brick, enhancing the heat insulation performance. Table 6 summarizes the geometrical details of CHD and FHD models. The 2D layout and the 3D design of the bricks are presented in Figure 5a,b, respectively.

Table 6. Details of CHD and FHD brick models.

Brick Model	Number of Holes	Hole Area (mm^2)	Hole Concentration Ratio (%)
CHD	11	490.625	28
FHD	10	425	23

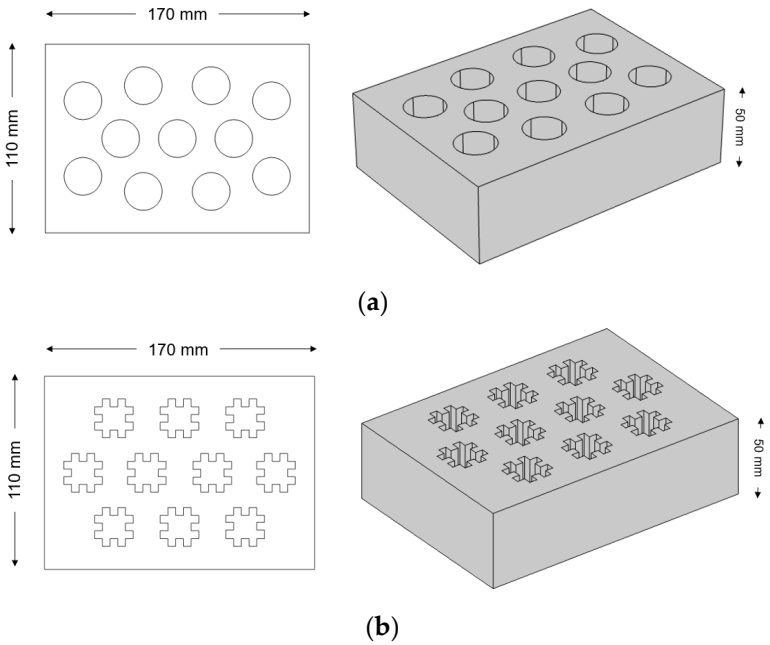

Figure 5. Hollow brick models: (**a**) CHD and (**b**) FHD.

2.2.2. FEA-Based Mechanical Analysis

Definition of the Problem

To preliminarily recognize the influence of the hollow design pattern on the mechanical performance of the brick, it was necessary to build a numerical FEA model, allowing a mechanical analysis of the component until the cracking state. The Structural Mechanics Module in COMSOL Multiphysics software was used for the calculation of the mechanical response of the hollow blocks under uniaxial compressive load regime. The numerical analysis consisted of simulating a static force-controlled compressive test, recording the stress–strain relationship and the mechanical parameters (compressive strength and modulus of elasticity) as a function of the brick's material and inner design. For this purpose, a compressive-load function (*CLF*) was defined as follows (Equation (1)):

$$CLF = 0.5 \times \xi \quad (1)$$

where 0.5 (MPa) is the unit load recommended by the current European technical standard [43] for mechanical testing on brick masonry, and ξ is a multiplier parameter that defines the analysis resolution depending on the concrete mix implemented in the model. By considering the strength values obtained from the material characterization (*Part 1*), the following measurement ranges were selected: $0 < \xi < 30$ per 100 values and $0 < \xi < 5$ per 50 values for REF and RuC-based bricks, respectively). During the analysis, ξ gradually varied, simulating the application of an incremental compressive load perpendicular to the holes plain. The simulation reached convergence when the computed failure of the block occurred. For this purpose, a non-linear model was implemented in COMSOL. Compared to a linear elastic analysis, in which it is assumed that Hooke's law governs the material behavior and the stresses involved are relatively smaller than the brick strength [44], the non-linear modeling is able to trace the complete response of the component from the elastic range, through cracking and crushing, up to complete failure [45]. This method was successfully used for decades by structural engineers for analysis and strengthening of masonry units [44].

Mathematical Modeling

The micromechanics and the failure behavior of the brick were modeled by adopting the Willam–Warnke (WW) yield criterion. The WW failure surface can be written as a tri-parametric criterion, in accordance with Equation (2):

$$\frac{F(\sigma_{xp}, \sigma_{yp}, \sigma_{zp})}{\sigma_f} - S(\sigma c,\ \sigma t, \sigma bc) \geq 0 \quad (2)$$

where F is the function of the principal stress state (σ_{xp}, σ_{yp}, and σ_{zp}); S is the failure surface depending on σ_c, σ_t, and biaxial compressive strength (σ_{bc}); and σ_f is the uniaxial crushing strength (MPa). The graphical representation of failure surface in 3D principal stress space is illustrated by Figure 6, where parameters η, r_1, and r_2 refer to the relative magnitudes of principal stresses on the octahedral plane [46].

Cracking happens when the principal stress in any direction lies outside the failure surface. Brick failure occurs if all the principal stresses are compressive and lie outside the WW surface [44].

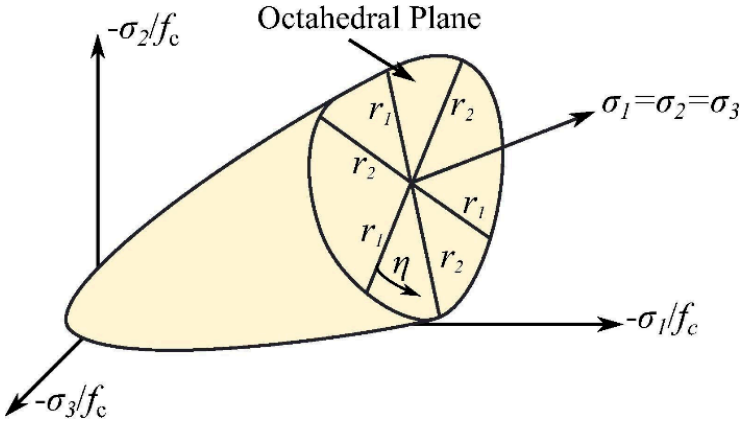

Figure 6. Three-dimensional WW failure surface in principal stress space (Reprinted with the permission from Ref. [46]. 2018, Elsevier Ltd.). In this representation, σ_1, σ_1, σ_3, and f_c are the three principal stresses and the uniaxial crushing strength, respectively.

Material Properties

The properties of the concrete mixes used in the FEA-based mechanical assay were taken from the laboratory tests described in *Part 1* of the manuscript and are listed below (Table 7):

Table 7. Material input properties for FEA-based mechanical investigation on brick models.

REF Concrete Mix			
Property	***Value***	***Property Group***	***Evaluation***
Density	2186 kg/m^3	Basic	Experimental
Porosity	21.39%	Basic	Experimental
Elastic modulus	1.62 GPa	Basic	Experimental
Poisson's ratio (ν)	0.32	Basic	$\nu = 0.0895 + 0.0063 \times \sigma_c$ [47]
Compressive strength	35.89 MPa	WW model	Experimental
Tensile strength	11.06 MPa	WW model	Experimental
Biaxial compressive strength	43.07 MPa	WW model	$\sigma_{bc} = 1.2 \times \sigma_c$ [44]
RuC Concrete Mix			
Property	***Value***	***Property Group***	***Evaluation***
Density	1281 kg/m^3	Basic	Experimental
Porosity	22.82%	Basic	Experimental
Elastic modulus	0.24 GPa	Basic	Experimental
Poisson's ratio (ν)	0.12	Basic	$\nu = 0.0895 + 0.0063 \times \sigma_c$ [45]
Compressive strength	4.93 MPa	WW model	Experimental
Tensile strength	1.65 MPa	WW model	Experimental
Biaxial compressive strength	5.92 MPa	WW model	$\sigma_{bc} = 1.2 \times \sigma_c$ [44]

Boundary Conditions

The boundary conditions selected in the analyses (Figure 7) involved a "boundary load" condition on the upper surface of the brick, applying a pressure defined by *CLF* (see Equation (1)). For the other boundaries of the model, the displacement in X, Y, and Z directions was constrained by setting "Prescribed displacement" equal to 0. With this

condition, the translations and rotations of the selected boundary, along a specific spatial direction, are disabled.

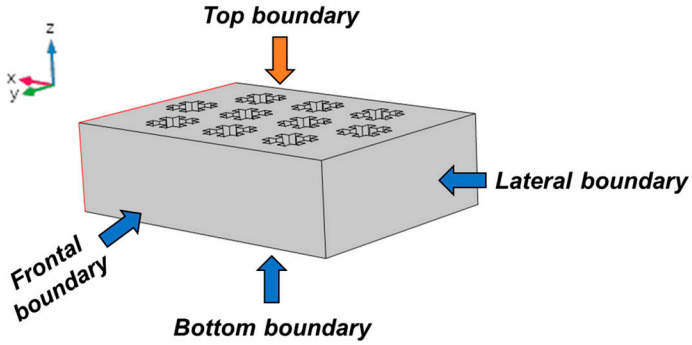

Boundary	Condition	Equation
Top	Boundary load	*CLF*
Lateral	Prescribed displacement in x direction	$u_{0x} = 0$
Frontal	Prescribed displacement in y direction	$u_{0y} = 0$
Bottom	Prescribed displacement in z direction	$u_{0z} = 0$

Figure 7. Schematic of the boundary conditions adopted in the FEA-based mechanical analysis.

A tetrahedral-shaped mesh was used for the numerical analysis. A "fine" element size (minimum mesh element size 3.5 mm and maximum mesh element size 28 mm) was chosen for meshing to achieve a good compromise among the results' accuracy and computational effort. Figure 8 illustrates the changes in WW damage index distribution on the brick surface for CHD (Figure 8a) and FHD (Figure 8b) models as ξ, varies.

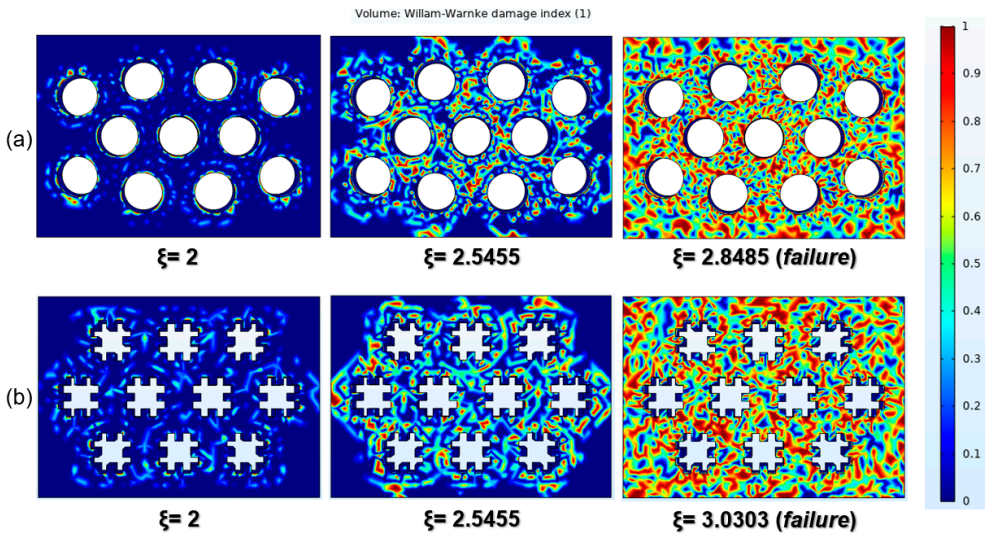

Figure 8. WW damage index distribution in (**a**) CHD model and (**b**) FHD model, considering RuC mix as constituent material.

2.2.3. FEA-Based Acoustic Analysis

Definition of the Problem

To explore the acoustic performance of the brick designs, a 2D FEA model was established through the Pressure Acoustic Module of COMSOL. The analysis aimed to characterize the absorption properties—more specifically, acoustic absorption coefficient (α)—of the hollow bricks in terms of sound frequency.

Mathematical Modeling

Two kinds of domains existed in the numerical model (Figure 9): (1) the background sound pressure field (Domain 1), which supplied a normal-incidence sound wave on the brick; and (2) the brick domain (Domain 2), which consisted of the air domain for the perforation holes and the concrete material matrix described by the Delany–Bazley (DB) poro-acoustic model. The DB model includes an empirical formulation for estimating acoustic impedance of porous materials. The acoustic impedance (Z_a) and wave-number (k) of the sound waves in a porous medium mainly depend on the frequency and on the static airflow resistivity (R_f) of the material. The expression of Z_a and k are as follows (Equations (3) and (4)):

$$Z_a = \rho_0 \times c_0 \left[1 + 0.057 \times \left(\frac{\rho_0 \times f}{R_f} \right)^{-0.754} - i0.087 \times \left(\frac{\rho_0 \times f}{R_f} \right)^{-0.732} \right] \quad (3)$$

$$k = \frac{2\pi f}{c_0} \times \left[1 + 0.0978 \times \left(\frac{\rho_0 \times f}{R_f} \right)^{-0.700} - i0.189 \times \left(\frac{\rho_0 \times f}{R_f} \right)^{-0.595} \right] \quad (4)$$

where ρ_0 is the air density (kg/m^3), c_0 is the sound velocity in air (m/s), f is the sound frequency (Hz), and i is the imaginary unit.

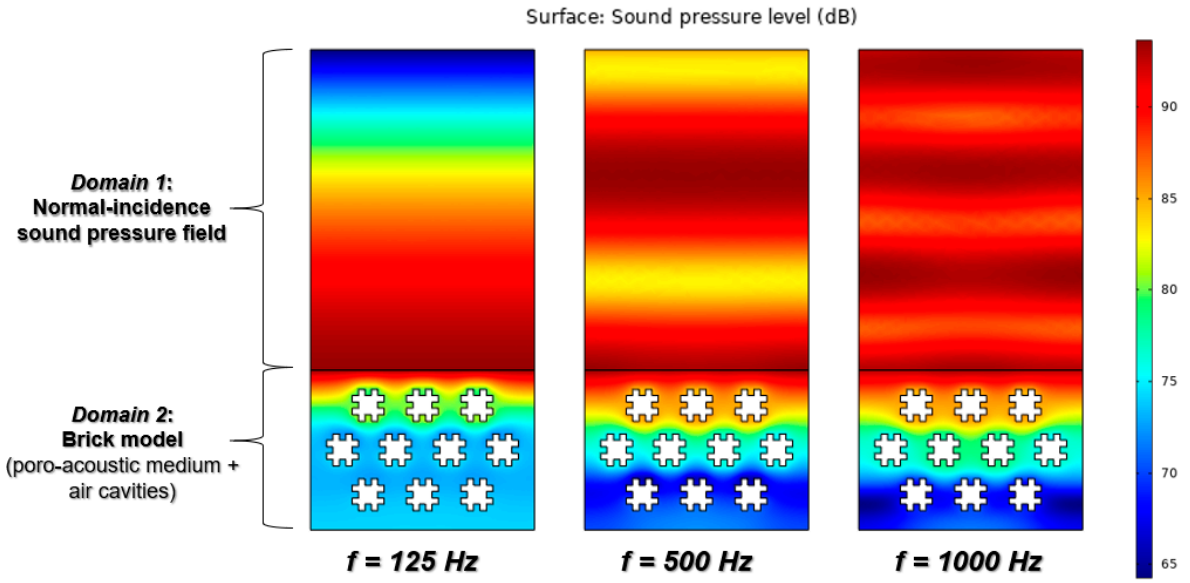

Figure 9. FEA-based acoustic model: sound-pressure-level variation as function of frequency in FHD brick, considering RuC mix as constituent material.

The incident background pressure field (P_i) is given as follows (Equation (5)):

$$P_i = e^{-i(k \cdot x)} \quad (5)$$

where k is the wave vector defining the propagation of the incident sound wave. The pressure, P, solved in the model is the total field, and the scattered field (P_{scat}) is given as $P_{scat} = P - P_i$. The α-coefficient, which represents the ratio of the absorbed and incident energy, is defined as follows (Equation (6)):

$$\alpha = 1 - |R|^2 \quad (6)$$

where R is the pressure reflection coefficient that gives the ratio of P_{scat} and P_{inc}. In the simulation, α-coefficient for CHD and FHD bricks was analyzed at different frequencies

(up to 1000 Hz), in accordance with the permitted working range of the impedance tube used in the experimental validation.

Material Properties

The input parameters for concrete mixes required from the FEA model are presented in Table 8. The air-cavity domain was modeled by adopting the value available in COMSOL's material library.

Table 8. Material input properties for FEA-based acoustic investigation on brick models.

REF Concrete Mix			
Property	***Value***	***Property Group***	***Evaluation***
Density	2186 kg/m^3	Basic	Experimental
Porosity	21.39%	Basic	Experimental
Acoustic flow resistivity	13,872 N × s× m^{-4}	DB model	Experimental
RuC Concrete Mix			
Property	***Value***	***Property Group***	***Evaluation***
Density	1281 kg/m^3	Basic	Experimental
Porosity	22.82%	Basic	Experimental
Acoustic flow resistivity	19,862 N × s× m^{-4}	DB model	Experimental

Boundary Conditions

As to boundary conditions, the lateral boundaries are all set as rigid walls, owing to the periodicity of unit cells for normal sound incidence, and the bottom of the brick domain is also rigid according to reproduce the common test configuration in sound absorption measurements. Normal-sized tetrahedral mesh (minimum mesh element size of 0.375 mm and maximum mesh element size of 83.8 mm) was selected in the study.

2.3. Part 3: Hollow-Brick Production and Testing

2.3.1. Fabrication of the Brick Mold

A custom-made polypropylene (PP) vessel was employed as a master mold. Circular and fractal-shaped columns were implanted on the mold's base to realize the cavities in the brick prototypes. To accurately reproduce the geometry of the holes, especially in the case of fractal configuration, the columns were cut from a slab of high-density polystyrene (HDPS) by a computerized numerical control (CNC) milling machine (Falcon 1500, Valmec, Pescara, Italy). The cutting parameters are reported in Table 9. Figure 10 elucidates some phases of the cutting operations.

Table 9. Cutting parameters selected for CNC cutting of high-density polystyrene columns.

Cutter Type	**Cutter Diameter**	**Cutting Depth**	**Spindle speed**	**Feed Rate**
End mill	3 mm	2 mm	5000 rpm	30 mm/s

The correct alignment of the columns on the mold's base was made possible through the fabrication of masks that exactly reproduced the hollow surface of the designed bricks. Tailored cardboard masks (Figure 10a) were produced by high-precision laser-cutting technology (Figure 10b), using a Birio 1000 laser cutter (Birio, Naples, Italy). After positioning and gluing the columns, we removed the guide-masks were, and the mold was left to settle to allow the complete fixing of the columns on the vessel's base The completed and ready-to-use brick molds (FHD and CHD configurations) are illustrated in Figure 11c,d, respectively.

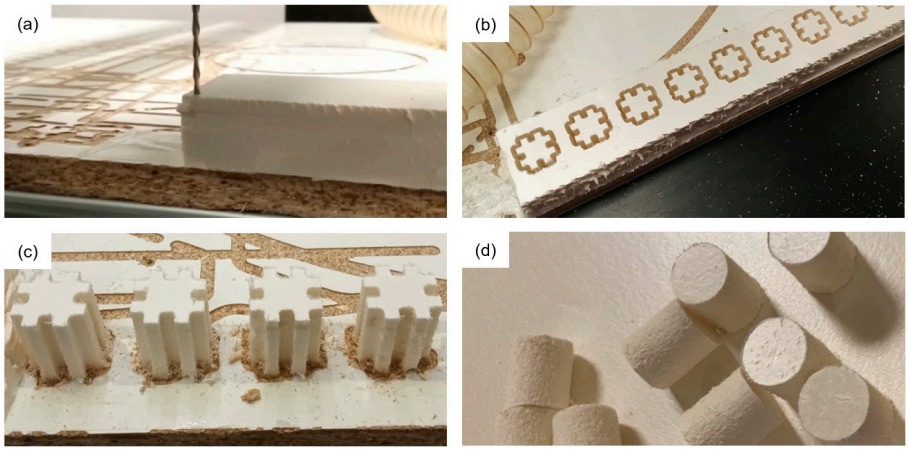

Figure 10. CNC cutting operation: (**a**) end mill, (**b**) array of fractal designs after cutting, and extraction of the (**c**) fractal and (**d**) circular columns.

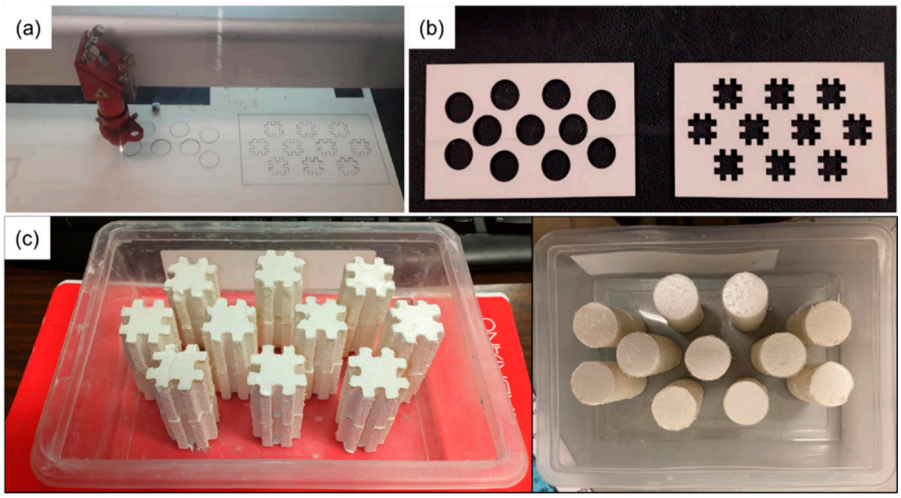

Figure 11. (**a**) Laser cutting of the guide-masks, (**b**) CHD and FHD guide masks, and (**c**) mold brick for FHD and CHD design.

2.3.2. Casting and Bricks Manufacturing

The concrete mixes preparation, casting procedure, and curing method followed the same protocol implemented in Section 2.1.2. After 28 days of curing, the bricks were demolded and the columns were removed both manually and by chemical etching with pure acetone. Then the surface of the brick specimens was polished by a diamond saw. For each brick design (CHD and FHD) and concrete mix (Figure 12), three replicates were produced.

2.3.3. Testing

The brick samples were mechanically characterized by compressive test (Figure 13a), using a Zwick-Roell Z150 (Zwick-Roell Group, Ulm, Germany) universal machine with a 150 kN load cell. The pre-load and loading rate were set to 20 N and 5 mm/min, respectively. Two brick specimens were tested for each combination (concrete material + inner design).

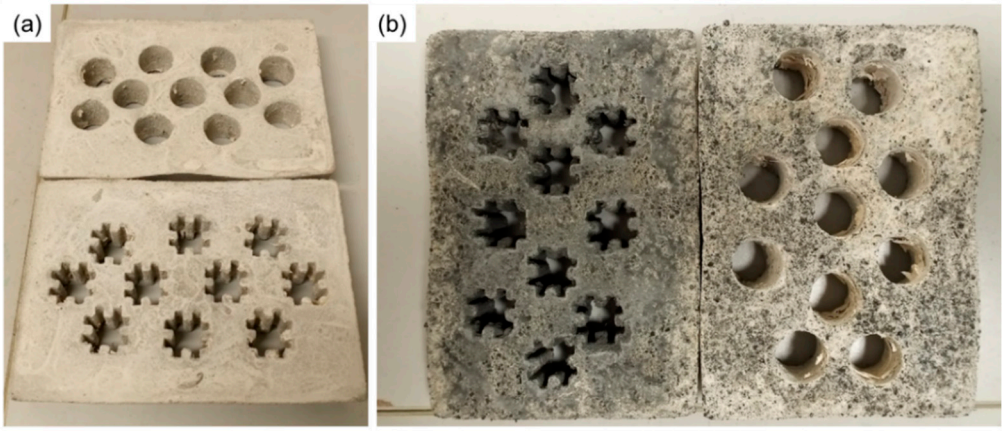

Figure 12. CHD and FHD hollow-brick prototypes: (**a**) REF mix and (**b**) RuC mix.

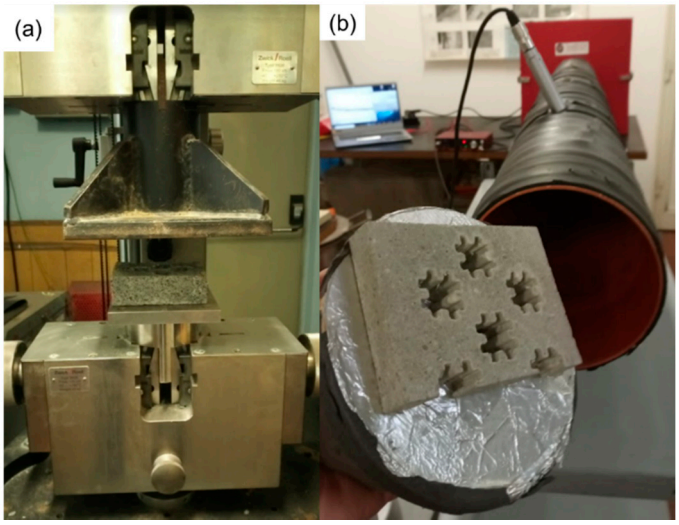

Figure 13. Experimental configurations for hollow brick characterization: (**a**) compressive test and (**b**) sound-absorption test.

The sound-absorption properties of the bricks were experimentally investigated by means of the impedance tube system by applying the standing wave ratio method (ASTM C384-95 standard [48]). The testing principle can be found in detail in Reference [35]. The measuring system included a 190 cm–long (L) Poly (vinyl chloride) (PVC) tube with an inner diameter (D) of 16 cm, a sound source (MPA30BT loudspeaker, Behringer, Willich, Germany), a $\frac{1}{4}$" condenser microphone (ECM800, Behringer, Willich, Germany), a Scarlett 2i4 audio interface (Focusrite, High Wycombe, UK), and Room EQ Wizard software (GIK Acoustic, Atlanta, GA, USA) test software. The sound source was mounted at one end of the tube, emitting a sine wave acoustic signal. Half-brick sample is placed at the other end fixed on a reflective termination (Figure 13b). The microphone moved along the length of the tube during the test, recording the sound pressure level at various frequencies. According to this system, the normal incidence α-coefficient was determined by Equation (7):

$$\alpha\,(f) = 1 - \left|\frac{SWR - 1}{SWR + 1}\right|^2 \tag{7}$$

where the standing wave ratio (SWR) index is defined as the ratio between the maximum and minimum sound pressure level values (in dB) measured along the tube for each acoustic frequency investigated. For the tube used in this study, the maximum operating frequency

was 1270 Hz. Then α-measurements were performed in third-octave bands at 125, 250, 500, and 1000 Hz

3. Results

3.1. FEA-Based Mechanical Analysis

The results of the mechanical FEA study are presented in Figure 14a (load–strain curves) and Figure 14b (WW damage index–load curves).

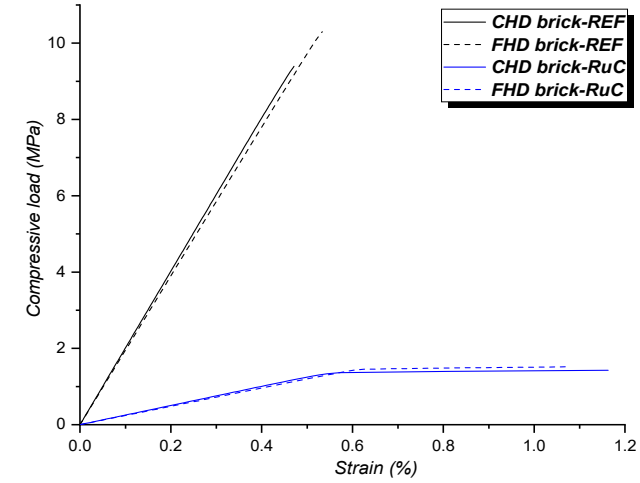

(**a**)

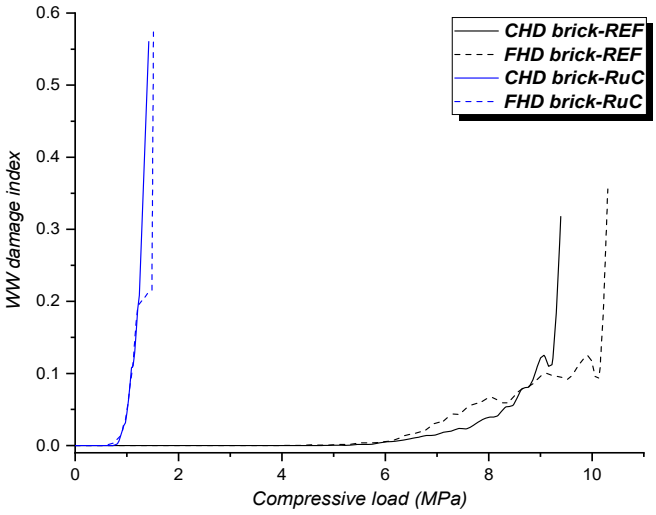

(**b**)

Figure 14. FEA-based mechanical results: (**a**) load–strain curves and (**b**) WW damage index–strain curves.

Regardless of the hollow brick design, a clear difference in mechanical behavior between the investigated concrete mixes can be observed. The FEA mechanical model implemented in this work faithfully reproduces the clear difference in the stress–strain relationship between ordinary and rubberized concrete. The former showed the typical brittle characteristic of ordinary cementitious materials. By considering RuC mix properties, the curve changes toward a more ductile behavior, showing lower mechanical strength and larger deformations compared to the plain concrete sample under the same loading conditions. From this evidence, it can be deduced that the features of the rubberized mix would be favorable in optimizing the strain capacity and, thus, the energy-absorption ability of the brick element. Therefore, an improvement to conventional concrete in terms

of attained vibro-acoustic performance could be achieved [49], representing an attractive requirement for building applications. In addition to yielding at lower compressive loads, the brick prototypes in RuC mix experienced a higher damage index than those modeled with REF properties, reflecting the strength vulnerability of the rubberized mixes compared to plain concrete.

When analyzing the effect of the hollow configuration, we can see that slight differences were noted between CHD and FHD in terms of elasto-mechanical characteristics. Cavities' geometry had little influence on the mechanical stiffness of the brick model. For the REF mix, the computed elastic moduli (E_{FEA}) were 2.01 GPa for CHD and 1.95 GPa for FHD. For the RuC mix, E_{FEA}-values were 0.25 GPa and 0.24 GPa. The fractal design performed better in terms of mechanical strength. The simulated compressive strengths (σ_c^{FEA}) of the REF-modeled brick were 9.39 MPa and 10.30 MPa for CHD and FHD bricks, respectively. The σ_c^{FEA} values of the RuC-modeled brick were 1.42 MPa and 1.51 MPa for CHD and FHD bricks, respectively. Overall, an increase in mechanical-strength properties of 7% (RuC mix) and 10% (REF mix) was achieved when passing from CHD to FHD configurations. No supporting works in the literature are available on the mechanical influence of this type of fractal-like cavity to corroborate the results obtained. However, some research work verified that structural components topologically optimized with fractal geometries gained significantly in terms of load-bearing capacity [50,51]. The damage level of the brick model would seem to be less affected by the cavities' geometry. With the same material properties, the fractal design provided slightly higher WW indices than the circular configuration, while showing greater strength performance. The fractal cavity contains internal square hollow shapes, where their sharp edges would induce more stress concentration than the circular hole. This effect, although potentially deleterious to the mechanical performance of the brick, is well-balanced by the lower hole concentration ratio in FHD arrangement, which therefore exposes a greater load-bearing strength to the applied stress.

3.2. FEA-Based Acoustic Analysis

In addition to evaluating the acoustic response of the brick models as a function of the constituent concrete material and type of hollow pattern, an FEA acoustic simulation was also used to predict the noise attenuation characteristics in low-frequency regimes. Low-frequency sound absorption for noise mitigation remains challenging because the slow fluctuation of low-frequency acoustic waves leads to poor interaction between materials or structures and the viscous air medium, resulting in inefficient dissipation of sound energy [52]. Moreover, the fundamental frequencies of most engineering and civil structures are usually below 50 Hz; therefore, their attenuation must be addressed to avoid unwanted vibro-acoustic phenomena [53]. The low-frequency acoustic performances are difficult to analyze experimentally. Common measurement methods, including impedance tube or reverberation room, provide working ranges strictly related to the dimensions of the measuring apparatus. For instance, the minimum admitted frequency ($f_{min} \propto \frac{c_0}{L-D}$) of the impedance tube device used in this research was 150 Hz, thus not allowing accurate measurements in the low-frequency band. In this regard, the FEA model implemented in this work was also used to analyze the sound-absorbing properties of the modeled brick in this acoustic region of great engineering interest.

The low-frequency acoustic spectrum (Figure 15a) highlights the weakest sound-absorbing ability ($\alpha < 0.20$) and a negligible influence of the internal design of the brick on the acoustic performance. The constituent concrete material, on the other hand, provides a certain effect within 60 Hz. The physical–acoustic properties of RuC mix would seem to confer better attenuation performance than those of REF mix. The considerable increase in R_f following the replacement of sand with GWTR (see discussion in Section 2.1.3) could be the key factor in the brick prototype's higher low-frequency performance. FEA results find good agreement with previous studies [53,54] wherein the improved low-frequency noise-suppression capacity of rubber–concrete mixes has been demonstrated. At around

60 Hz, an inversion point was detected: α-curves grew continuously, converging to a value close to 0.9 (around 1000 Hz), indicating that high frequencies are more easily attenuated. In the high-frequency acoustic range (Figure 15b), the physical–acoustic properties of the REF mix ensured higher sound absorption rates than those of rubberized concrete. Above 500 Hz, passing from a circular hollow internal geometry to a fractal one, a very slight improvement in acoustic performance is appreciated by FEA modeling. It can be hypothesized that the different acoustic behavior of the two brick models is due to the cavity resonance sound-absorption mechanism. According to the thermo-viscous acoustic theory of irregular cavities, sound propagation in the air is related to the displacement and movement speed of small particles. When the shape of the sound-absorbing cavity is more complex, the surfaces are more reflective, and the smaller particles need to travel more distance. Therefore, the sound waves are reflected more frequently in the irregular space of the cavity wall, which consumes more sound energy and improves the sound absorption ability [55].

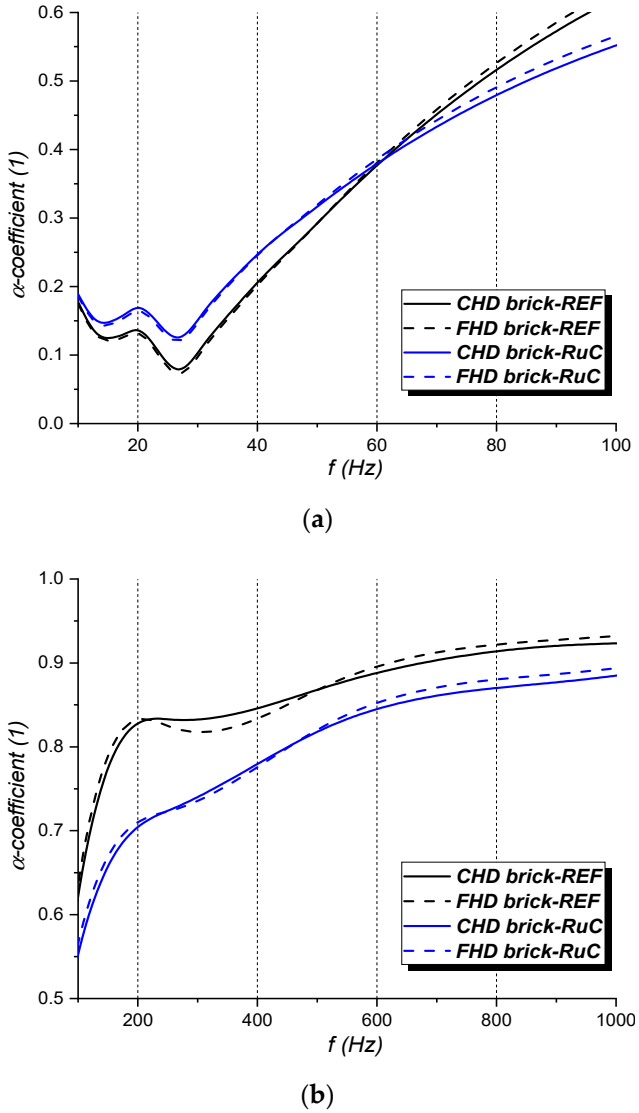

Figure 15. FEA-based acoustic results: (**a**) low-frequency α-coefficient curves and (**b**) middle-high-frequency α-coefficient curves.

3.3. Experimental Mechanical Testing

In accordance with the results predicted by the simulation, the mechanical tests reveal the marked difference in the load–strain relationship (Figure 16) between REF (brittle

behavior) and RuC (ductile behavior) mixes, indicating, for the latter, a predictable deterioration in strength and an increase in post-peak strain capacity because of the influence of rubber particles. The curves, normalized with respect to the holes concentration ratio, also allow us to detect the difference between the hollow designs under study. Regardless of the type of concrete mix, the FHD sample provided higher stiffness and compressive strength than the CHD brick. The numerical analysis (Figure 14a) reports a similar trend in the compressive behavior of the bricks but underestimates the mechanical resistance values. Indeed, there is an average level of agreement between experimental and simulated compressive strength of 45% and 55% for REF and RuC-based bricks, respectively. This discrepancy can be attributed to several approximations considered in the building of the COMSOL model:

- The FEA model considers the material as homogeneous, neglecting the composite nature of the cementitious formulations under study and, therefore, the contribution of mineral (sand) and polymeric (GWTR) aggregates on the mechanical behavior of the model, including interface interactions, stress distribution, deformation mechanisms induced by the different nature of the aggregates, etc.;
- Some fundamental input properties for the WW failure criterion (such as ν and σ_{bc}) were obtained indirectly from constitutive models and may not reflect the real mechanical behavior of the material;
- Dimensional variations between the digital model and real brick prototype due to the hygrometric shrinkage of the material, the geometric accuracy of the cavities, and surface roughness can inevitably affect the mechanical response of the samples.

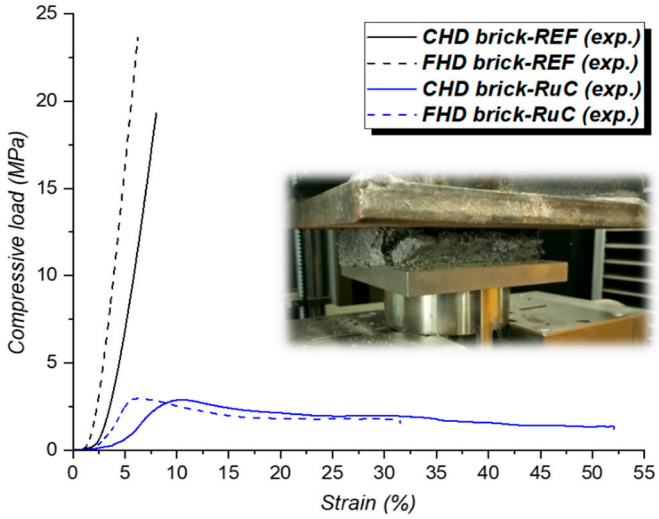

Figure 16. Experimental load–strain curves.

Figure 17 elucidates the average values of compressive strength obtained from mechanical testing. REF-based bricks satisfy the strength requirement for load-bearing masonry units. The minimum compressive strength value of 11.7 MPa is necessary for this case, as reported in the ASTM C90 standard [56]. The strengths dramatically decrease in the rubberized hollow brick, as expected. Both the bricks provide mechanical strengths very close to the minimum ASTM requirements [57] for non-load bearing hollow concrete masonry blocks (minimum strength requirement of 3.45 MPa). Furthermore, the histograms clearly show the increase in mechanical performance induced by the fractal-shaped hollow pattern. From CHD to FHD, increments of 22% and 18% are detected by considering REF mix and RuC mix, respectively, confirming the efficiency of fractal design on the mechanical behavior of the brick. To determine the best brick solutions from the structural point of view, a structural efficiency index (*SEI*) is defined. This value is computed as the ratio

between the compressive strength (σ_c^{exp}), which is obtained from the experimental testing, and its weight (Equation (8)):

$$SEI = \frac{\sigma_c^{exp}}{Weight} \quad (8)$$

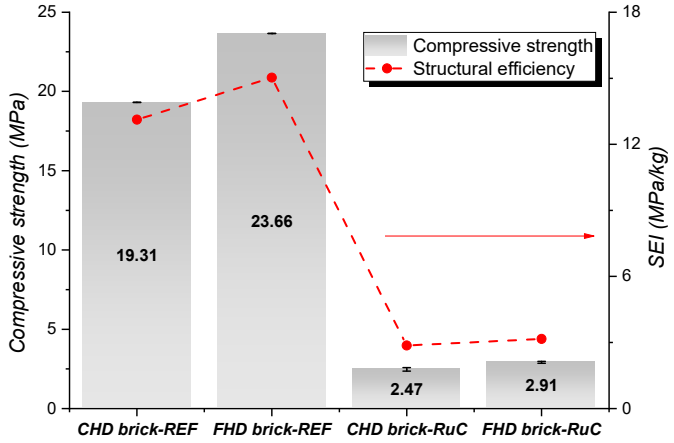

Figure 17. Compressive strength and *SEI* values for developed hollow bricks.

The greater *SEI* values found in FHD designs indicate the higher overall structural effectiveness of the block, which behaves better from a structural and handling point of view [19]. The results achieved represent a noteworthy starting point for researchers. With careful optimization and engineering of both GWTR–concrete mix and structural design, it is possible to reach a highly eco-sustainable brick (0% natural aggregates) with a mechanical performance suitable for applications in construction.

3.4. Experimental Acoustic Testing

The experimental sound–absorption curves (α vs. f) are presented in Figure 18.

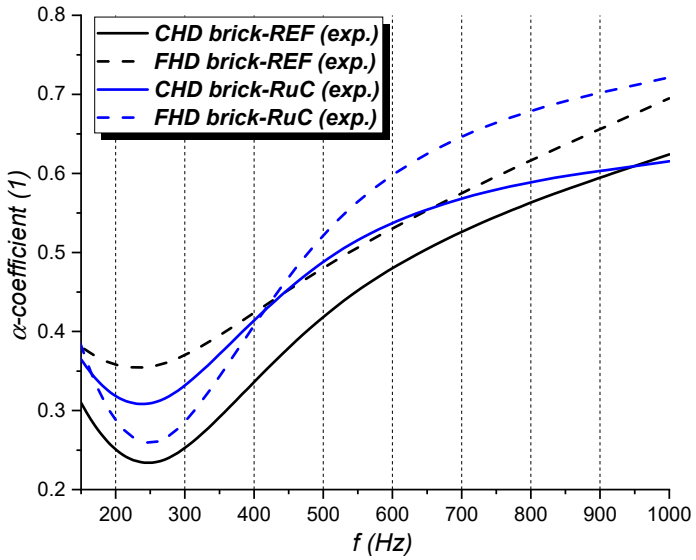

Figure 18. Experimental sound–absorption curves (α vs. f).

Considering the trend of α-curves, the experimental results follow with fairly good agreement the numerical analysis (Figure 15b). The acoustic absorption of the hollow brick prototypes tends to have the highest α-values as the frequency increases. In contrast to the simulation, however, lower attenuation levels are recorded. At 1000 Hz, α-coefficient varies between 0.62 (CHD brick-RuC) and 0.72 (FHD brick-RuC), compared to values close to

0.90 detected in the acoustic-based FEA modeling. The inconsistency between simulation and experimental analysis is primarily attributable to the poro-acoustic model adopted to describe the sound–material interaction and the acoustic impedance provided by the cementitious medium. DB's model was derived for fibrous sound-absorbing materials, such as glass wool and rock wool [58] and could induce uncertainties in the prediction of the acoustic response of concrete-based materials. In addition, the model required a limited number of input acoustic data referring to the material, affecting the accurate prediction of its real sound-absorbing performance. In this regard, it will be advisable, in future works, to implement more complete acoustic models suitable for concrete, including Neithalath's model [59] and Kim and Lee's model [60], which need a greater number of acoustic parameters describing the material's performance.

The experimental α-coefficients indicate a very good acoustic performance of the developed hollow bricks. Referring to the classification presented by Fediuk et al. [61], the samples exhibit sound-absorbing levels in the range of aerated and foamed concretes (α = 0.15–0.75), which represent the major solutions in building noise-attenuation interventions. Furthermore, the sound-absorbing ability of the proposed rubberized bricks is significantly higher than the experimental results obtained by Mohammed et al. [15], which found α-values less than 0.25 in concrete hollow blocks loaded with different amounts (10%, 25%, and 50%) of tire crumb rubber. In good agreement with FEA, the experimental α-curves highlight the better acoustic performance of FHD design above 400 Hz for both cement mixes. The sharpest incremental rate in sound absorption, moving from CHD to FHD, is recorded for RuC-based samples: +13% at 500 Hz and +18% at 1000 Hz. In the same frequency band, the GWTR–cement mix yields superior acoustic attenuation capacities compared to REF material, regardless of the internal geometry of the brick, indicating the acoustic functionality induced by the polymeric aggregate on the concrete's damping [62]. The improved acoustic efficiency of fractal-shaped cavities coupled with the sound abatement peculiarities deriving from the tire aggregate would provide attractive solutions for acoustic dampening at medium–high frequencies, which are of particular interest concerning the mitigation of traffic and urban-deriving noise [63].

4. Conclusions

In this study, ground waste tire rubber and fractal-shaped cavities were combined with the purpose of producing eco-friendly and lightweight hollow concrete bricks with improved acoustic efficiency and acceptable strength requirements for non-structural applications. The rubberized concrete mix was prepared by using two rubber fractions (0–1 mm rubber powder and 1–3 mm rubber granules) as a total aggregate. Firstly, its physical and mechanical properties were experimentally characterized and compared with an ordinary concrete mix (0% rubber) taken as a reference. A finite element analysis was implemented to build predictive models for the mechanical and acoustic absorption behavior of two kinds of brick models based on circular (traditional geometry) and Minkowski-like fractal cavities. Hollow-brick prototypes were manufactured and tested, evaluating the influence of constituent materials (reference and rubberized mixes) and inner hollow design on their mechanical and acoustic performance. The results revealed the following main findings:

- Regardless of the concrete mix, the fractal hollow pattern provides a significant improvement in the engineering performance of the brick in terms of mechanical strength, structural efficiency, and acoustic absorption over 500 Hz. Considering the rubber–cement mix as a constituting brick's material, an increase of 18% in compressive strength and 1000 Hz sound absorption coefficient can be achieved, moving from circular to fractal hole designs.
- Circular and fractal design bricks made up of ordinary concrete mix satisfy the minimum ASTM strength for load-bearing masonry units. A rubber–concrete mix involves a predictable loss in mechanical strength properties. However, the compressive strengths of rubberized blocks were very close to ASTM requirements for non-load-bearing applications.

- The samples investigated can be considered as "good" concrete sound absorbers. The rubber-functionalized cement mix yielded superior acoustic attenuation capacities compared to the reference material, regardless of the internal geometry of the brick, indicating the positive influence induced by the polymeric aggregates on the concrete's sound-absorbing efficiency.
- From the numerical analysis by finite element method, the physical–acoustic parameters of the investigated rubberized mixes would seem to predict better attenuation performances to the brick, even at low frequencies, which are noise events of great interest in engineering field.

In summary, the present study has proven that fractal geometries and waste aggregates can be successfully integrated into brick technology to obtain eco-friendlier solutions with enhanced structural and acoustic behavior. As a future trend, we plan to propose a careful optimization of the rubber–cement mix design to achieve mechanical performances that are fully within the strength requirements for lightweight masonry applications. In this regard, it will also be necessary to refine the finite element predictive models and to strengthen the connection between simulation and experiment for a more accurate optimization of the material and component's design.

Author Contributions: Conceptualization, M.V., M.S. and S.L.; methodology, M.V., M.S., A.S., L.F. and R.M.; software, M.S. and A.S.; validation M.S. and A.S.; investigation, M.S., A.S. and R.M.; resources, M.V., L.F. and S.L.; writing—original draft preparation, M.S. and A.S.; writing—review and editing, M.V., L.F., R.M. and S.L.; supervision, M.V., L.F. and S.L.; project administration, M.V. All authors have read and agreed to the published version of the manuscript.

Funding: This research received no external funding.

Data Availability Statement: Not applicable.

Acknowledgments: The authors would like to thank the technical staff of Saperi&Co center staff for supporting the design and production of the brick molds.

Conflicts of Interest: The authors declare no conflict of interest.

References

1. Valentini, F.; Dorigato, A.; Rigotti, D.; Pegoretti, A. Evaluation of the role of devulcanized rubber on the thermomechanical properties of expanded ethylene-propylene diene monomers composites. *Polym. Eng. Sci.* **2021**, *61*, 767–779. [CrossRef]
2. Shu, X.; Huang, B. Recycling of waste tire rubber in asphalt and portland cement concrete: An overview. *Constr. Build. Mater.* **2014**, *67*, 217–224. [CrossRef]
3. Eldin, N.N.; Senouci, A.B. Engineering properties of rubberized concrete. *Can. J. Civ. Eng.* **1992**, *19*, 912–923. [CrossRef]
4. Miller, N.M.; Tehrani, F.M. Mechanical properties of rubberized lightweight aggregate concrete. *Constr. Build. Mater.* **2017**, *147*, 264–271. [CrossRef]
5. Turatsinze, A.; Garros, M. On the modulus of elasticity and strain capacity of self-compacting concrete incorporating rubber aggregates. *Resour. Conserv. Recycl.* **2008**, *52*, 1209–1215. [CrossRef]
6. Ghizdăveț, Z.; Ștefan, B.M.; Nastac, D.; Vasile, O.; Bratu, M. Sound absorbing materials made by embedding crumb rubber waste in a concrete matrix. *Constr. Build. Mater.* **2016**, *124*, 755–763. [CrossRef]
7. Zhang, B.; Poon, C.S. Sound insulation properties of rubberized lightweight aggregate concrete. *J. Clean. Prod.* **2018**, *172*, 3176–3185. [CrossRef]
8. Guo, J.; Huang, M.; Huang, S.; Wang, S. An experimental study on mechanical and thermal insulation properties of rubberized concrete including its microstructure. *Appl. Sci.* **2019**, *9*, 2943. [CrossRef]
9. Richardson, A.; Coventry, K.; Dave, U.; Pienaar, J. Freeze/thaw performance of concrete using granulated rubber crumb. *J. Green Build.* **2011**, *6*, 83–92. [CrossRef]
10. Gerges, N.N.; Issa, C.A.; Fawaz, S.A. Rubber concrete: Mechanical and dynamical properties. *Case Stud. Constr. Mater.* **2018**, *9*, e00184. [CrossRef]
11. Jie, X.U.; Yao, Z.; Yang, G.; Han, Q. Research on crumb rubber concrete: From a multi-scale review. *Constr. Build. Mater.* **2020**, *232*, 117282. [CrossRef]
12. Thorat, P.K.; Papal, M.; Kacha, V.; Sarnobat, T.; Gaikwad, S. Hollow concrete blocks-A new trend. *Int. J. Eng. Res.* **2015**, *5*, 9–26.
13. Turgut, P.; Yesilata, B. Physico-mechanical and thermal performances of newly developed rubber-added bricks. *Energy Build.* **2008**, *40*, 679–688. [CrossRef]

14. Yüksek, İ.; Öztaş, S.K.; Tahtalı, G. The evaluation of fired clay brick production in terms of energy efficiency: A case study in Turkey. *Energy Effic.* **2020**, *13*, 1473–1483. [CrossRef]
15. Mohammed, B.S.; Hossain, K.M.A.; Swee, J.T.E.; Wong, G.; Abdullahi, M. Properties of crumb rubber hollow concrete block. *J. Clean. Prod.* **2012**, *23*, 57–67. [CrossRef]
16. Fraile-Garcia, E.; Ferreiro-Cabello, J.; Defez, B.; Peris-Fajanes, G. Acoustic Behavior of Hollow Blocks and Bricks Made of Concrete Doped with Waste-Tire Rubber. *Materials* **2016**, *9*, 962. [CrossRef]
17. Al-Fakih, A.; Wahab, M.A.; Mohammed, B.S.; Liew, M.S.; Zawawi, N.A.W.A.; As' ad, S. Experimental study on axial compressive behavior of rubberized interlocking masonry walls. *J. Build. Eng.* **2020**, *29*, 101107. [CrossRef]
18. Lourenço, P.B.; Vasconcelos, G.; Medeiros, P.; Gouveia, J. Vertically perforated clay brick masonry for loadbearing and non-loadbearing masonry walls. *Constr. Build. Mater.* **2010**, *24*, 2317–2330. [CrossRef]
19. Del Coz Díaz, J.J.; Nieto, P.G.; Rabanal, F.Á.; Martínez-Luengas, A.L. Design and shape optimization of a new type of hollow concrete masonry block using the finite element method. *Eng. Struct.* **2011**, *33*, 1–9. [CrossRef]
20. Al-Tamimi, A.S.; Al-Osta, M.A.; Al-Amoudi, O.S.B.; Ben-Mansour, R. Effect of geometry of holes on heat transfer of concrete masonry bricks using numerical analysis. *Arab. J. Sci. Eng.* **2017**, *42*, 3733–3749. [CrossRef]
21. Sassine, E.; Cherif, Y.; Dgheim, J.; Antczak, E. Investigation of the mechanical and thermal performances of concrete hollow blocks. *SN Appl. Sci.* **2020**, *2*, 1–17. [CrossRef]
22. Valente, M.; Sambucci, M.; Sibai, A.; Musacchi, E. Multi-physics analysis for rubber-cement applications in building and architectural fields: A preliminary analysis. *Sustainability* **2020**, *12*, 5993. [CrossRef]
23. Kim, H.; Hong, J.; Pyo, S. Acoustic characteristics of sound absorbable high performance concrete. *Appl. Acoust.* **2018**, *138*, 171–178. [CrossRef]
24. Sapoval, B.; Haeberlé, O.; Russ, S. Acoustical properties of irregular and fractal cavities. *J. Acoust. Soc. Am.* **1997**, *102*, 2014–2019. [CrossRef]
25. Hébert, B.; Sapoval, B.; Russ, S. Experimental study of a fractal acoustical cavity. *J. Acoust. Soc. Am.* **1999**, *105*, 1567–1574. [CrossRef]
26. Godbold, O. Investigating Broadband Acoustic Absorption Using Rapid Manufacturing. Ph.D. Thesis, Loughborough University, Loughborough, UK, 2008.
27. *EN 1097-7*; Tests for Mechanical and Physical Properties of Aggregates—Part 7: Determination of the Particle Density of Filler—Pycnometer Method. UNI Standards: Milan, Italy, 2008.
28. *DIN 51701*; Testing of Solid Fuels; Sampling and Sample Preparation, Sample Preparation. DIN Standards: Berlin, Germany, 2007.
29. Sambucci, M.; Valente, M.; Sibai, A.; Marini, D.; Quitadamo, A.; Musacchi, E. Rubber-Cement Composites for Additive Manufacturing: Physical, Mechanical and Thermo-Acoustic Characterization. In Proceedings of the Second RILEM International Conference on Concrete and Digital Fabrication, Eindhoven, The Netherlands, 6–9 July 2020; Springer: Cham, Switzerland, 2020; pp. 113–124. [CrossRef]
30. Sambucci, M.; Valente, M. Influence of Waste Tire Rubber Particles Size on the Microstructural, Mechanical, and Acoustic Insulation Properties of 3D-Printable Cement Mortars. *Civ. Eng. J.* **2021**, *7*, 937–952. [CrossRef]
31. Valente, M.; Sambucci, M.; Chougan, M.; Ghaffar, S.H. Reducing the emission of climate-altering substances in cementitious materials: A comparison between alkali-activated materials and Portland cement-based composites incorporating recycled tire rubber. *J. Clean. Prod.* **2022**, *333*, 130013. [CrossRef]
32. *ASTM D792*; Standard Test Methods for Density and Specific Gravity (Relative Density) of Plastics by Displacement. ASTM International: West Conshohocken, PA, USA, 1958.
33. *ASTM C 1202*; Standard Test. Method for Electrical Indication of Concrete's Ability to Resist Chloride Ion Penetration. ASTM International: West Conshohocken, PA, USA, 2019.
34. Ingard, K.U.; Dear, T.A. Measurement of acoustic flow resistance. *J. Sound Vib.* **1985**, *103*, 567–572. [CrossRef]
35. Sambucci, M.; Valente, M. Ground Waste Tire Rubber as a Total Replacement of Natural Aggregates in Concrete Mixes: Application for Lightweight Paving Blocks. *Materials* **2021**, *14*, 7493. [CrossRef]
36. Assaggaf, R.A.; Ali, M.R.; Al-Dulaijan, S.U.; Maslehuddin, M. Properties of concrete with untreated and treated crumb rubber–A review. *J. Mater. Res. Technol.* **2021**, *11*, 1753–1798. [CrossRef]
37. Si, R.; Guo, S.; Dai, Q. Durability performance of rubberized mortar and concrete with NaOH-Solution treated rubber particles. *Constr. Build. Mater.* **2017**, *153*, 496–505. [CrossRef]
38. Rezaifar, O.; Hasanzadeh, M.; Gholhaki, M. Concrete made with hybrid blends of crumb rubber and metakaolin: Optimization using Response Surface Method. *Constr. Build. Mater.* **2016**, *123*, 59–68. [CrossRef]
39. Geethamma, V.G.; Asaletha, R.; Kalarikkal, N.; Thomas, S. Vibration and sound damping in polymers. *Resonance* **2014**, *19*, 821–833. [CrossRef]
40. Sambucci, M.; Cecchini, F.; Nanni, F.; Pucacco, G.; Valente, M. Metamateriali fonoassorbenti sviluppati via 3D printing per interventi acustici nel settore automotive. *Riv. Ital. Di Acust.* **2020**, *44*, 1–23.
41. *EN 771-1*; Specification for Masonry Units—Part 1: Clay Masonry Units. UNI Standards: Milan, Italy, 2015.
42. Nagy, B.; Orosz, M. Optimized Thermal Performance Design of Filled Ceramic Masonry Blocks. *AMM* **2015**, *797*, 174–181. [CrossRef]

43. *EN 1996-1-1*; Eurocode 6—Design of Masonry Structures—Part 1-1: General Rules for Reinforced and Unreinforced Masonry Structures. UNI Standards: Milan, Italy, 2013.
44. Hejazi, M.; Soltani, Y. Parametric study of the effect of hollow spandrel (Konu) on structural behaviour of Persian brick masonry barrel vaults. *Eng. Fail. Anal.* **2020**, *118*, 104838. [CrossRef]
45. Lourenço, P.B. Computations on historic masonry structures. *Prog. Struct. Eng. Mater.* **2002**, *4*, 301–319. [CrossRef]
46. Kumar, P.; Srivastava, G. Effect of fire on in-plane and out-of-plane behavior of reinforced concrete frames with and without masonry infills. *Constr. Build. Mater.* **2018**, *167*, 82–95. [CrossRef]
47. Sideris, K.K.; Manita, P.; Sideris, K. Estimation of ultimate modulus of elasticity and Poisson ratio of normal concrete. *Cem. Concr. Compos.* **2004**, *26*, 623–631. [CrossRef]
48. *ASTM C384-95*; Standard Test Method for Impedance and Absorption of Acoustical Materials by the Impedance Tube Method. ASTM International: West Conshohocken, PA, USA, 1998.
49. El-Khoja, A. Mechanical, Thermal and Acoustic Properties of Rubberised Concrete Incorporating Nano Silica. Ph.D. Thesis, University of Bradford, Bradford, UK, 2019.
50. Nguyen-Van, V.; Wu, C.; Vogel, F.; Zhang, G.; Nguyen-Xuan, H.; Tran, P. Mechanical performance of fractal-like cementitious lightweight cellular structures: Numerical investigations. *Compos. Struct.* **2021**, *269*, 114050. [CrossRef]
51. Khoshhesab, M.M.; Li, Y. Mechanical behavior of 3D printed biomimetic Koch fractal contact and interlocking. *Extrem. Mech. Lett.* **2018**, *24*, 58–65. [CrossRef]
52. Cai, X.; Guo, Q.; Hu, G.; Yang, J. Ultrathin low-frequency sound absorbing panels based on coplanar spiral tubes or coplanar Helmholtz resonators. *Appl. Phys. Lett.* **2014**, *105*, 121901. [CrossRef]
53. Cheng, Z.; Shi, Z. Vibration attenuation properties of periodic rubber concrete panels. *Constr. Build. Mater.* **2014**, *50*, 257–265. [CrossRef]
54. Thakur, A.; Senthil, K.; Sharma, R.; Singh, A.P. Employment of crumb rubber tyre in concrete masonry bricks. *Mater. Today Proc.* **2020**, *32*, 553–559. [CrossRef]
55. Xie, S.; Yang, S.; Yan, H.; Li, Z. Sound absorption performance of a conch-imitating cavity structure. *Sci. Prog.* **2022**, *105*, 00368504221075167. [CrossRef] [PubMed]
56. *ASTM C 90*; Standard Specification for Load-Bearing Concrete Masonry Units. ASTM International: West Conshohocken, PA, USA, 2014.
57. *ASTM C129*; Standard Specification for Nonloadbearing Concrete Masonry Units. ASTM International: West Conshohocken, PA, USA, 2017.
58. Komatsu, T. Improvement of the Delany-Bazley and Miki models for fibrous sound-absorbing materials. *Acoust. Sci. Technol.* **2008**, *29*, 121–129. [CrossRef]
59. Neithalath, N.; Marolf, A.; Weiss, J.; Olek, J. Modeling the influence of pore structure on the acoustic absorption of enhanced porosity concrete. *J. Adv. Concr. Technol.* **2005**, *3*, 29–40. [CrossRef]
60. Kim, H.K.; Lee, H.K. Acoustic absorption modeling of porous concrete considering the gradation and shape of aggregates and void ratio. *J. Sound Vib.* **2010**, *329*, 866–879. [CrossRef]
61. Fediuk, R.; Amran, M.; Vatin, N.; Vasilev, Y.; Lesovik, V.; Ozbakkaloglu, T. Acoustic Properties of Innovative Concretes: A Review. *Materials* **2021**, *14*, 398. [CrossRef]
62. Bala, A.; Gupta, S. Thermal resistivity, sound absorption and vibration damping of concrete composite doped with waste tire Rubber: A review. *Constr. Build. Mater.* **2021**, *299*, 123939. [CrossRef]
63. Tie, T.S.; Mo, K.H.; Putra, A.; Loo, S.C.; Alengaram, U.J.; Ling, T.C. Sound absorption performance of modified concrete: A review. *J. Build. Eng.* **2020**, *30*, 101219. [CrossRef]